HHS Public Access

Author manuscript

Radiographics. Author manuscript; available in PMC 2017 July 04.

Published in final edited form as:

Radiographics. 2016 ; 36(1): 162–175. doi:10.1148/rg.2016150030.

Benign Conditions That Mimic Prostate Carcinoma: MR Imaging Features with Histopathologic Correlation[1]

Yu Xuan Kitzing, MBBS, **Adilson Prando, MD**, **Celi Varol, MBBS**, **Gregory S. Karczmar, PhD**, **Fiona Maclean, MBBS**, and **Aytekin Oto, MD**

Departments of Medical Imaging (Y.X.K.) and Urology (C.V.), Macquarie University Hospital, Sydney, Australia; Department of Radiology, Hospital Vera Cruz, Campinas, Brazil (A.P.); Department of Radiology, University of Chicago, Chicago, Ill (G.S.K., A.O.); and Douglass Hanly Moir Pathology, Sydney, Australia (F.M.)

Abstract

Multiparametric magnetic resonance (MR) imaging combines anatomic and functional imaging techniques for evaluating the prostate and is increasingly being used in diagnosis and management of prostate cancer. A wide spectrum of anatomic and pathologic processes in the prostate may masquerade as prostate cancer, complicating the imaging interpretation. The histopathologic and imaging findings of these potential mimics are reviewed. These entities include the anterior fibromuscular stroma, surgical capsule, central zone, periprostatic vein, periprostatic lymph nodes, benign prostatic hyperplasia (BPH), atrophy, necrosis, calcification, hemorrhage, and prostatitis. An understanding of the prostate zonal anatomy is helpful in distinguishing the anatomic entities from prostate cancer. The anterior fibromuscular stroma, surgical capsule, and central zone are characteristic anatomic features of the prostate with associated low T2 signal intensity due to dense fibromuscular tissue or complex crowded glandular tissue. BPH, atrophy, necrosis, calcification, and hemorrhage all have characteristic features with one or more individual multiparametric MR imaging modalities. Prostatitis constitutes a heterogeneous group of infective and inflammatory conditions including acute and chronic bacterial prostatitis, infective and noninfective granulomatous prostatitis, and malacoplakia. These entities are associated with variable clinical manifestations and are characterized by the histologic hallmark of marked inflammatory cellular infiltration. In some cases, these entities are indistinguishable from prostate cancer at multiparametric MR imaging and may even exhibit extraprostatic extension and lymphadenopathy, mimicking locally advanced prostate cancer. It is important for the radiologists interpreting prostate MR images to be aware of these pitfalls for accurate interpretation.

---

[1]Recipient of a Certificate of Merit award for an education exhibit at the 2014 RSNA Annual Meeting. Received February 21, 2015; revision requested May 11 and received May 30; accepted July 31. For this journal-based SA-CME activity, the author A.O. has provided disclosures (see p 174); all other authors, the editor, and the reviewers have disclosed no relevant relationships.

Address correspondence to Y.X.K., Department of Radiology, Royal Prince Alfred Hospital, Missenden Rd, Camperdown 2050, NSW, Australia (yuxuan.kitzing@sswahs.nsw.gov.au).

***Disclosures of Conflicts of Interest.*—A.O.** *Activities related to the present article:* disclosed no relevant relationships. *Activities not related to the present article:* grant from Philips Healthcare; consultant for Guerbet. *Other activities:* disclosed no relevant relationships.

Introduction

Prostate cancer was the most common new cancer diagnosis in the United States in 2014 and is the cause of 10% of cancer-related deaths in American men (1). Prostate cancer diagnosis is based on random transrectal ultrasonography (US)–guided prostate biopsies prompted by an elevated serum prostate-specific antigen (PSA) level or positive digital rectal examination. With the development of advanced magnetic resonance (MR) imaging techniques, MR imaging is increasingly playing a role in the clinical pathways of detection, local staging, active surveillance, and posttreatment follow-up. With the increasing influence that MR imaging has on clinical decision making, it is important to be aware of the potential pitfalls in imaging interpretation.

In this review, we discuss the multiparametric MR imaging findings and histologic correlations of a range of anatomic and pathologic findings that mimic prostate carcinoma.

Histopathologic Features of Prostate Carcinoma

Prostatic adenocarcinoma ranges from a recognizable glandular pattern to cords, nests, or sheets of cells. The Gleason grade is used by pathologists to grade the histologic pattern of carcinoma cellular arrangement (2). Addition of the primary and secondary grade patterns gives rise to the Gleason score, which is a major predictor of disease outcome. With a higher Gleason grade, there is less resemblance of the adenocarcinoma to the normal glandular formation.

The malignant acini are small and closely spaced, with little intervening stroma. The glands may form a papillary or cribriform pattern, and the cells have larger nuclei in general (Fig 1a). This histologic appearance contrasts with that of the normal prostate peripheral zone, which consists of glands with single-layered columnar epithelium with abundant background supporting stroma (Fig 1b). The key histologic features of prostate carcinoma pertinent to MR imaging are increased cellular density, decreased luminal volume, reduced extracellular space, and neoangiogenesis.

MR Imaging Appearance of Typical Prostate Carcinoma

State-of-the-art MR imaging of the prostate incorporates anatomic and functional techniques in a multiparametric approach. The addition of functional imaging techniques increases the sensitivity and specificity in identification of clinically significant prostate cancer. A multiparametric MR imaging protocol that includes T2-weighted imaging, diffusion-weighted (DW) imaging, and dynamic contrast-enhanced (DCE) imaging is widely embraced throughout the world as the routine prostate MR imaging protocol (3) (Table 1).

T2-weighted imaging delineates the anatomic details of the prostate carcinoma, with clear differentiation between the peripheral and transition zones. Prostate cancer appears as focal low signal intensity against the background of the high-signal-intensity glandular tissue (Fig 1c). Tumor in the transition zone has a lenticular shape with an “erased charcoal” appearance (4,5).

DW imaging is reflective of the motion of water in the imaged tissue. This correlates with properties that include cellular density, membrane permeability, and space between cells (6). Prostate cancer appears bright on DW images and dark on ADC maps, indicating restricted diffusion. A low ADC, reflective of greater diffusion restriction, has been shown to correlate with a higher Gleason score (7,8) (Fig 1d).

DCE imaging consists of a series of axial T1-weighted gradient-echo sequences covering the prostate during and after intravenous bolus contrast material injection. Tumor angiogenesis leads to neovessels that are highly irregular and tortuous with increased permeability (9). This is proposed as the basis for the early rapid enhancement and subsequent contrast enhancement washout or plateau observed in prostate carcinoma (10–12). The data can be assessed qualitatively, semiquantitatively with enhancement curves, or quantitatively with pharmacokinetic parameter mapping (Fig 1e).

Mimics of Prostate Carcinoma at MR Imaging

Anterior Fibromuscular Stroma

The anterior fibromuscular stroma is a band of fibromuscular tissue anterior to the transition zone, contiguous with the bladder smooth muscle and the skeletal muscle of the sphincter (13). It is also continuous with the pseudocapsule of the prostate. It covers the anterior and anterolateral surface of the glandular prostate. Histologically, it comprises dense irregular connective tissue with a large amount of smooth muscle fibers interposed with adjacent skeletal muscle fibers of the urethra (Fig 2a).

The anterior fibromuscular stroma has markedly low T2 signal intensity and low ADC due to its compact muscle and fiber composition (14). The anterior fibromuscular stroma varies in its prominence among individuals. It is less prominent in men with increased age and gland size, likely due to the compressive effect of benign prostatic hyperplasia (BPH) (15). When it is bulky, it may mimic anterior tumor in its lentiform morphology, low T2 signal intensity, and low ADC (Fig 2b). The distinguishing feature of normal anterior fibromuscular stroma is its midline and symmetric position. The anterior fibromuscular stroma is often hypovascular, possibly due to its fibrous nature (Fig 2c).

Surgical Capsule

At the junction between the transition zone and peripheral zone, there is a concentrically placed band of fibromuscular and compressed glandular tissue that demarcates the transition zone. It is more pronounced in the setting of BPH (Fig E1a [online]). This band of fibromuscular demarcation has been described in the older surgical literature as a “surgical capsule” (16). It forms part of the network of supporting fibromuscular tissue in the prostate, including the anterior fibromuscular stroma. Poor definition of the surgical capsule on T2-weighted images can sometimes be seen adjacent to a transition zone cancer.

A normal surgical capsule has low signal intensity on both T2-weighted images and ADC maps due to the dense compacted fibromuscular tissue (Fig E1b–E1d [online]). It can mimic a small tumor that is growing within the confines of the lateral peripheral zone in a linear fashion. The anatomic morphology is linear rather than masslike.

Central Zone

The central zone is a layer of tissue that surrounds the ejaculatory ducts from the level of the prostatic base down to the verumontanum (17). It is most prominent at the base of the prostate and has a conical shape, with its apex at the verumontanum. Embryologically, the central zone originates from the wolffian duct, whereas the transition zone is a derivative of the urogenital sinus. The central zone accounts for 25% of the total prostate volume but almost 40% of the epithelium because of its high epithelial-to-stromal ratio (18). Its volume starts to decrease in a gradual fashion after the age of 35 years due to reduced mean glandular activity, reduction of acinar size, and epithelial atrophy (19).

Compared to the peripheral zone, the glands of the central zone are larger and more complex, with tall columnar cells and papillary folding (Fig 3a) (18). There is also increased apposition of the glands with denser stroma. Central zone cancers are rare, accounting for 0.5%–2.5% of all prostate cancer and 3%–8% of index tumors (20). They are usually associated with a high incidence of seminal vesicle invasion, extracapsular extension, high Gleason grade, and early biochemical failure after attempted curative surgery (20).

The normal central zone appears homogeneously hypointense on T2-weighted images and dark on ADC maps in patients aged 42–84 years (Fig 3b, 3c) (21,22). With these characteristics, it can mimic prostate cancer. A symmetric appearance of the central zone and its expected location can be helpful to differentiate it from prostate cancer, but in 20% of cases, the central zone may be asymmetric (21). Enlargement of the transition zone can lead to compression of the central zone and increased displacement to the base. At DCE imaging, the central zone has been shown to be associated with type 1 (progressive) and type 2 (early enhancement and plateau) rather than type 3 (early enhancement and washout) enhancement curve types (22). It is important for radiologists to be familiar with the normal appearance of the central zone so as not to “overcall” it as prostate cancer.

Periprostatic Vein

The periprostatic venous plexus is closely associated with the pseudocapsule of the prostate and is also known as the Santorini venous plexus (Fig E2a [online]). It lies predominantly anterior and lateral to the prostate. The calibers of the veins vary between individuals and are larger in younger patients and smaller glands (15). At MR imaging, periprostatic veins are mostly tubular rounded structures with high T2 signal intensity (14). However, the veins can have low signal intensity on T2-weighted images and ADC maps, depending on the velocity and turbulence of the blood movement (Fig E2b [online]) (23).

Prominent periprostatic veins with low T2 and ADC signal intensity may be difficult to differentiate from intraprostatic lesions, particularly at the apex. At the apex, there is sparseness of the pseudocapsule with intermixing of the periprostatic supporting tissue and glandular tissue (24). The partial voluming of the axial sections and the horizontal oblique orientation of the veins at the apex also contribute to the difficulty in delineating between intra- and extraprostatic structures. The veins enhance avidly with the DCE sequence. Unlike tumor, the veins tend to have a linear morphology (Fig E2c [online]). Careful examination of the other planes as well as the axial sections above and below the venous

structure can help demonstrate the continuity with the remainder of the periprostatic venous plexus.

Periprostatic Lymph Nodes

Periprostatic lymph nodes are not common and are detected in 4.4% of specimens from radical prostatectomy (Fig E3a [online]) (25). They are most commonly located at the base of the prostate laterally or posterolaterally. Pathologic analysis of the prostatectomy specimen has shown malignant involvement of the periprostatic lymph node in 15% of cases (26). The prognostic significance of isolated periprostatic lymph node involvement versus pelvic lymph node involvement is uncertain.

Similar to lymph nodes elsewhere, periprostatic lymph nodes have rounded morphology with low T2 signal intensity and marked diffusion restriction (Fig E3b, E3c [online]). The degree of diffusion restriction does not imply metastatic involvement. On the low-spatial-resolution DW images and ADC maps, periprostatic lymph nodes may appear to be intraprostatic structures. The anatomic T2-weighted imaging helps define their periprostatic location and likely cause.

Benign Prostatic Hyperplasia

BPH is enlargement of the transition zone and is characterized by hyperplasia of the prostatic stromal and epithelial cells, resulting in formation of large discrete nodules. The histologic subtypes of BPH nodules include glandular proliferation/dilatation and fibromuscular proliferation of the stroma (Fig 4a). BPH gives a heterogeneous appearance to the transition zone on T2-weighted images (27).

BPH nodules may be hypo-, iso-, or hyperintense on T2-weighted images, depending on the ratio of glandular to stromal tissue. It has been shown that high signal intensity is due to hyperplastic glandular elements, which are filled with secretion, and the presence of cystic ectasia. These cystic BPH nodules do not mimic prostate cancer. However, mixed and stromal BPH nodules can demonstrate low T2 signal intensity due to the presence of prominent sclerotic, fibrous, or muscular elements and may mimic transition zone cancer (Fig 4b) (28–30). Stromal BPH nodules also demonstrate restricted diffusion on DW images and early enhancement on DCE images, similar to prostate cancer (Fig 4c, 4d) (28). Recognition of the different histologic subtypes of BPH is important for radiologists to improve the diagnosis of transition zone cancer.

Homogeneous low signal intensity (erased charcoal sign), ill-defined margins, lack of capsule, lenticular shape, and invasion of the anterior fibromuscular stroma are the MR imaging findings suggestive of transition zone cancer on T2-weighted images (4). Stromal hyperplasia tends to be more well defined, with a rounded encapsulated appearance. Despite some overlap between the ADCs of transition zone cancer and stromal hyperplasia, the ADC can help differentiate transition zone cancer from glandular hyperplasia and, to a lesser degree, stromal hyperplasia (28). The role of DCE imaging in this differentiation is limited.

Rarely, BPH nodules can also be seen in the peripheral zone and mimic prostate cancer (31). In our experience, their well-defined rounded appearance and internal heterogeneity at T2-

weighted imaging may hint at the diagnosis of BPH and allow its differentiation from prostate cancer (Fig E4 [online]).

Bacterial Prostatitis

Bacterial prostatitis can manifest as acute or chronic prostatitis. It has an estimated prevalence of 9.7% (32). Acute bacterial prostatitis is uncommon and more likely to occur in young men. It occurs from intraprostatic reflux of urine infected with organisms such as *Escherichia coli*, *Enterococcus*, and *Proteus* or from instrumentation such as prostatic biopsy. The cellular hallmark of acute prostatitis is an influx of neutrophils (Fig 5a).

Chronic bacterial prostatitis may result from undertreated acute prostatitis and recurrent infection but can also occur without prior history in older men with lower urinary tract obstruction. Routine cultures often do not allow identification of the common organism. Lymphocytes are seen in chronic prostatitis (Fig 6a), often accompanied by glandular atrophy. The clinical presentation of acute prostatitis tends to be a combination of both local and systemic symptoms. In comparison, chronic prostatitis tends to be more indolent, with lower urinary tract symptoms and no systemic symptoms (33).

Prostatitis can be diffuse or focal in morphology (Fig 5; see also Fig E5 [online]). At MR imaging, it tends to have low T2 signal intensity with mild to moderate diffusion restriction due to the increased inflammatory cellular infiltrates (Fig 5a, 5b). The degree of diffusion restriction in chronic prostatitis tends to be less than in prostate carcinoma (34). DCE imaging shows increased and early enhancement compared with normal prostate tissue, similar to prostate carcinoma (35). While bacterial prostatitis is most commonly visualized in the peripheral zone at MR imaging, it can also occur in the transition zone, where it may mimic the “erased charcoal” appearance of prostate carcinoma (Fig 6b–6d).

It is important to be aware that enlarged reactive lymph nodes may also be seen in the setting of acute prostatitis. A clinical history of urinary and/or sexual symptoms, fluctuating PSA level, or PSA response to antibiotics can alert the radiologist and the clinician to the possibility of prostatitis.

Granulomatous Prostatitis

Clinically, granulomatous prostatitis is often mistaken for prostate cancer. Five types are described: idiopathic (nonspecific and nonnecrotic), infective (specific, nonnecrotic or necrotic), iatrogenic (postsurgical), malacoplakia, and associated with systemic granulomatous disease (36).

Idiopathic granulomatous prostatitis is the most common type, making up 60%–77.7% of granulomatous prostatitis cases in reported series (36–38). It has no clear cause and no associated systemic diseases and is often self-limiting. Iatrogenic granulomatous prostatitis is the second most common type and relates to transurethral resection of the prostate or bladder as a result of reaction to altered epithelium and stroma from the intervention (36,38). Histologically, it is characterized by palisaded histiocytoid granulomas with central necrotizing or fibrinoid necrosis and surrounded by infiltrative eosinophils (39).

Sarcoidosis is an idiopathic multisystem noncaseating granulomatous disease with a predilection among African-Americans (40). Involvement of the prostate is rare, with only 14 cases reported in the literature (40,41). Most of the patients are asymptomatic with elevated PSA level. The histologic features are not specific, with the diagnosis based on clinical-radiologic correlation and exclusion of other granulomatous disease entities (42).

Infective Granulomatous Prostatitis—Infective granulomatous prostatitis can be caused by *Mycobacterium tuberculosis* (via hematogenous spread or direct extension from adjacent organs) or develop after intravesical bacillus Calmette-Guérin therapy for bladder cancer. It is characterized by well-formed granulomas with epithelioid cell and multinucleated giant cell infiltration with or without central necrosis (caseation) (Fig 7). Other rare infectious agents are *Treponema pallidum*, viruses (herpes zoster), and fungi (*Cryptococcus*, *Candida*, *Aspergillus*) (Fig E6 [online]) (43,44).

Nonnecrotic granulomatous prostatitis is highly cellular and may simulate prostate cancer at MR imaging. In the peripheral zone, it appears as an area of hypointensity on T2-weighted images associated with diffusion restriction and with moderate or marked enhancement on DCE images. In necrotic granulomatous prostatitis, central necrosis (caseation) has high signal intensity on T2-weighted images, with focal hyperintensity on high-*b*-value images, marked diffusion restriction, and total lack of enhancement on DCE images (45) (Fig 7). Florid granulomatous prostatitis may demonstrate extraprostatic extension. In patients with a histologic diagnosis of granulomatous prostatitis and prostate cancer, it is difficult to predict whether the findings of extraprostatic extension are secondary to prostate cancer or to granulomatous disease, since both entities may have a similar appearance at MR imaging (Fig 7a, 7b).

Patients with mycobacterial granulomatous prostatitis are mostly asymptomatic. Indurated prostate at digital rectal examination and elevated PSA level are features common to both prostate carcinoma and mycobacterial granulomatous prostatitis. Prediposing risk factors that should raise the possibility of mycobacterial granulomatous prostatitis include history of tuberculosis infection, bacillus Calmette-Guérin therapy, and immunosuppressive state (46,47). With treatment, the swelling of the prostate reduces and the caseous abscess cavity resolves (45). There may be residual fibrosis and calcification based on previously reported computed tomographic features of mycobacterial granulomatous prostatitis (48,49). In our experience, there are residual patchy areas of markedly low T2 signal intensity within the prostate due to a combination of calcification, fibrosis, and noncaseating necrosis.

Malacoplakia—Malacoplakia is a rare granulomatous inflammatory condition associated with recurrent infection. It predominantly affects the genitourinary tract, particularly the renal collecting system, and is more common in women than men. In men, it can rarely involve the prostate (50). The pathognomonic finding is granulomatous infiltration with Michaelis-Gutmann bodies, which may represent abnormality of intraphagosomal digestion of macrophages (Fig 8a) (51).

Owing to the inflammatory cellular infiltrate in malacoplakia, multiparametric MR imaging shows diffuse low T2 signal intensity, diffusion restriction, and hyperenhancement at DCE

imaging, thus simulating prostate cancer (Fig 8b–8d). Bulging and irregularity of the prostate capsule mimicking tumoral extraprostatic extension may also be present.

Atrophy

Atrophy is characterized by crowded glands with scant cytoplasm and crowding of nuclei compared to normal prostatic tissue. Histologic subtypes include simple, sclerotic with cyst formation, and post-atrophic hyperplastic. Focal atrophy, particularly the post-atrophic hyperplastic subtype, may mimic prostate malignancy at MR imaging due to its glandular crowding and complex glandular architecture (Fig 9a). Causes of atrophy include inflammation, radiation, antiandrogens, and chronic ischemia resulting from local arteriosclerosis.

There is a positive association between the extent of atrophy at biopsy and the total or free serum elevation of PSA level (52). This is possibly due to PSA release from damaged epithelial cells in atrophic acini. The atrophy may account for the elevated PSA level in the absence of prostate cancer. However, this benign and frequent histopathologic finding at prostate biopsy is not usually mentioned by the pathologists in their report.

Focal atrophy occurs more frequently in the peripheral zone and on multiparametric MR images appears as a focal or geographic appearance of low T2 signal intensity with moderate diffusion restriction and moderate enhancement on DCE images (Fig 9b–9d). The degree of diffusion restriction and tissue enhancement is usually less marked than with prostate cancer. In cases of geographic appearance, volume loss of affected tissue is usually present.

Necrosis

Necrosis can be seen following treated infective prostatitis as the florid inflammatory changes and abscesses resolve. Increasingly, it is also seen after focal therapy (radiofrequency ablation, cryoablation, high-intensity focused ultrasound, irreversible electroporation, laser ablation) for prostate carcinoma. Histologically, there is a central well-defined zone of coagulative necrosis of glands and stroma, with peripheral chronic inflammatory cellular infiltrate and atrophy (Fig 10a).

Necrosis shows low T2 signal intensity and diffusion restriction due to the coagulative necrosis with reduced water movement, as well as the adjacent inflammatory infiltrate and atrophy (Fig 10b–10d). There is absence of enhancement. The marked low T2 signal intensity and lack of enhancement are MR imaging features suggestive of necrosis and fibrosis. The T2 signal intensity is lower than that of tumor, possibly due to the fibrosis and early calcification. After focal therapy for prostate cancer, DCE imaging is useful for delineating the treatment zone and is the most sensitive technique for detection of recurrent disease (53).

Calcification

Calcification is seen within the prostate due to concreted prostatic secretions or calcified corpora amylacea (54). It is also seen adjacent to the prostate due to phlebolith in the

periprostatic venous plexus. While intraprostatic calcification can be related to lower urinary tract symptoms, in most cases it is asymptomatic and an incidental finding.

Owing to the diamagnetic effect of the calcium, calcification has low signal intensity on T2-weighted and ADC images (Fig E7 [online]). It is commonly seen at the junction between the transition zone and peripheral zone against the background of BPH. Lack of enhancement, persistent marked low signal intensity with the DW sequence at all *b* values, and the occasional low signal intensity with the T1-weighted sequence help confirm its nature.

Hemorrhage

Hemorrhage is commonly seen in the prostate after biopsy. It is more common in the peripheral zone than in the transition zone (55). Several studies have shown a mixed relationship between the amount of hemorrhage and the interval since biopsy (55,56). Most institutions advocate waiting 6–8 weeks after biopsy before performing MR imaging.

Hemorrhage can limit the ability of multiparametric MR imaging to delineate the extent or location of the tumor owing to the associated variably low T2 signal intensity. Depending on the age of the hemorrhage, it can also show diffusion restriction compared with the normal tissue and mimic tumor. In general, however, prostate cancer has lower ADC than benign peripheral zone hemorrhage (57). Hemorrhage is bright on T1-weighted images, which can limit qualitative interpretation of DCE images, with reduced delineation between the enhancing tumor foci and the background hemorrhagic high signal intensity. Subtraction images are useful to eliminate the background high signal intensity.

Areas of hemorrhage in the prostate after biopsy are suggestive of sampling during biopsy. Tumor has a lower rate of hemorrhage compared with normal tissue, reportedly 2%–10.5% (57,58). Prostate carcinoma is known to have lower levels of citrate, which has an anticoagulant effect (59). This may lead to faster resolution of hemorrhage within the tumor foci compared to hemorrhage within the normal peripheral zone. Areas of prostate without hemorrhage may indicate the sites of biopsy-proved tumor (Fig E8 [online]) (58). Correlation with the T1-weighted images would help reduce misinterpretation of hemorrhage-related changes with the other multiparametric MR imaging sequences.

Conclusion

Multiparametric MR imaging combines anatomic and functional imaging techniques for evaluation of prostatic carcinoma. Several normal anatomic findings and pathologic conditions of the prostate have multiparametric MR imaging characteristics that overlap with those of prostate carcinoma. Several of the mimics have histologic features similar to those of prostate carcinoma, with increased cellularity, reduced loose supporting stroma, and/or increased mean vascular density (Table 2). Even though a definitive diagnosis can be established only with histopathologic examination, awareness of these entities by the radiologists interpreting prostate MR images is crucial.

Supplementary Material

Refer to Web version on PubMed Central for supplementary material.

Abbreviations

ADC	apparent diffusion coefficient
BPH	benign prostatic hyperplasia
DCE	dynamic contrast-enhanced
DW	diffusion-weighted
H-E	hematoxylin-eosin
PSA	prostate-specific antigen

References

1. Siegel R, Ma J, Zou Z, Jemal A. Cancer statistics, 2014. CA Cancer J Clin. 2014; 64(1):9–29. [PubMed: 24399786]
2. Gleason DF. Classification of prostatic carcinomas. Cancer Chemother Rep. 1966; 50(3):125–128. [PubMed: 5948714]
3. Dickinson L, Ahmed HU, Allen C, et al. Magnetic resonance imaging for the detection, localisation, and characterisation of prostate cancer: recommendations from a European consensus meeting. Eur Urol. 2011; 59(4):477–494. [PubMed: 21195536]
4. Akin O, Sala E, Moskowitz CS, et al. Transition zone prostate cancers: features, detection, localization, and staging at endorectal MR imaging. Radiology. 2006; 239(3):784–792. [PubMed: 16569788]
5. Barentsz JO, Richenberg J, Clements R, et al. ESUR prostate MR guidelines 2012. Eur Radiol. 2012; 22(4):746–757. [PubMed: 22322308]
6. Padhani AR, Liu G, Koh DM, et al. Diffusion-weighted magnetic resonance imaging as a cancer biomarker: consensus and recommendations. Neoplasia. 2009; 11(2):102–125. [PubMed: 19186405]
7. Hambrock T, Somford DM, Huisman HJ, et al. Relationship between apparent diffusion coefficients at 3.0-T MR imaging and Gleason grade in peripheral zone prostate cancer. Radiology. 2011; 259(2):453–461. [PubMed: 21502392]
8. Turkbey B, Shah VP, Pang Y, et al. Is apparent diffusion coefficient associated with clinical risk scores for prostate cancers that are visible on 3-T MR images? Radiology. 2011; 258(2):488–495. [PubMed: 21177390]
9. Russo G, Mischi M, Scheepens W, De la Rosette JJ, Wijkstra H. Angiogenesis in prostate cancer: onset, progression and imaging. BJU Int. 2012; 110(11 Pt C):E794–E808. [PubMed: 22958524]
10. Hara N, Okuizumi M, Koike H, Kawaguchi M, Bilim V. Dynamic contrast-enhanced magnetic resonance imaging (DCE-MRI) is a useful modality for the precise detection and staging of early prostate cancer. Prostate. 2005; 62(2):140–147. [PubMed: 15389803]
11. Noworolski SM, Henry RG, Vigneron DB, Kurhanewicz J. Dynamic contrast-enhanced MRI in normal and abnormal prostate tissues as defined by biopsy, MRI, and 3D MRSI. Magn Reson Med. 2005; 53(2):249–255. [PubMed: 15678552]
12. Ren J, Huan Y, Wang H, et al. Dynamic contrast-enhanced MRI of benign prostatic hyperplasia and prostatic carcinoma: correlation with angiogenesis. Clin Radiol. 2008; 63(2):153–159. [PubMed: 18194690]
13. McNeal JE. Normal and pathologic anatomy of prostate. Urology. 1981; 17(suppl 3):11–16. [PubMed: 6163241]

14. Hricak H, Dooms GC, McNeal JE, et al. MR imaging of the prostate gland: normal anatomy. AJR Am J Roentgenol. 1987; 148(1):51–58. [PubMed: 3491523]
15. Allen KS, Kressel HY, Arger PH, Pollack HM. Age-related changes of the prostate: evaluation by MR imaging. AJR Am J Roentgenol. 1989; 152(1):77–81. [PubMed: 2783293]
16. Semple JE. Surgical capsule of the benign enlargement of the prostate: its development and action. BMJ. 1963; 1(5346):1640–1643. [PubMed: 13987912]
17. McNeal JE. The zonal anatomy of the prostate. Prostate. 1981; 2(1):35–49. [PubMed: 7279811]
18. McNeal JE. Normal histology of the prostate. Am J Surg Pathol. 1988; 12(8):619–633. [PubMed: 2456702]
19. McNeal, JE., Burroughs Wellcome, C. The prostate gland: morphology and pathobiology. Princeton, NJ: Burroughs Wellcome; 1983.
20. Cohen RJ, Shannon BA, Phillips M, Moorin RE, Wheeler TM, Garrett KL. Central zone carcinoma of the prostate gland: a distinct tumor type with poor prognostic features. J Urol. 2008; 179(5): 1762–1767. discussion 1767. [PubMed: 18343454]
21. Vargas HA, Akin O, Franiel T, et al. Normal central zone of the prostate and central zone involvement by prostate cancer: clinical and MR imaging implications. Radiology. 2012; 262(3): 894–902. [PubMed: 22357889]
22. Hansford BG, Karademir I, Peng Y, et al. Dynamic contrast-enhanced MR imaging features of the normal central zone of the prostate. Acad Radiol. 2014; 21(5):569–577. [PubMed: 24703469]
23. Rosenkrantz AB, Taneja SS. Radiologist, be aware: ten pitfalls that confound the interpretation of multiparametric prostate MRI. AJR Am J Roentgenol. 2014; 202(1):109–120. [PubMed: 24370135]
24. Ayala AG, Ro JY, Babaian R, Troncoso P, Grignon DJ. The prostatic capsule: does it exist? Its importance in the staging and treatment of prostatic carcinoma. Am J Surg Pathol. 1989; 13(1):21–27. [PubMed: 2909195]
25. Kothari PS, Scardino PT, Ohori M, Kattan MW, Wheeler TM. Incidence, location, and significance of periprostatic and periseminal vesicle lymph nodes in prostate cancer. Am J Surg Pathol. 2001; 25(11):1429–1432. [PubMed: 11684961]
26. Yuh B, Wu H, Ruel N, Wilson T. Analysis of regional lymph nodes in periprostatic fat following robot-assisted radical prostatectomy. BJU Int. 2012; 109(4):603–607. [PubMed: 21851536]
27. Grossfeld GD, Coakley FV. Benign prostatic hyperplasia: clinical overview and value of diagnostic imaging. Radiol Clin North Am. 2000; 38(1):31–47. [PubMed: 10664665]
28. Oto A, Kayhan A, Jiang Y, et al. Prostate cancer: differentiation of central gland cancer from benign prostatic hyperplasia by using diffusion-weighted and dynamic contrast-enhanced MR imaging. Radiology. 2010; 257(3):715–723. [PubMed: 20843992]
29. Kayhan A, Fan X, Oommen J, Oto A. Multi-parametric MR imaging of transition zone prostate cancer: imaging features, detection and staging. World J Radiol. 2010; 2(5):180–187. [PubMed: 21161033]
30. Schiebler ML, Tomaszewski JE, Bezzi M, et al. Prostatic carcinoma and benign prostatic hyperplasia: correlation of high-resolution MR and histopathologic findings. Radiology. 1989; 172(1):131–137. [PubMed: 2472644]
31. Oyen RH, Van de Voorde WM, Van Poppel HP, et al. Benign hyperplastic nodules that originate in the peripheral zone of the prostate gland. Radiology. 1993; 189(3):707–711. [PubMed: 7694310]
32. Nickel JC, Downey J, Hunter D, Clark J. Prevalence of prostatitis-like symptoms in a population based study using the National Institutes of Health chronic prostatitis symptom index. J Urol. 2001; 165(3):842–845. [PubMed: 11176483]
33. Ramakrishnan K, Salinas RC. Prostatitis: acute and chronic. Prim Care. 2010; 37(3):547–563. viii–ix. [PubMed: 20705198]
34. Gürses B, Tasdelen N, Yencilek F, et al. Diagnostic utility of DTI in prostate cancer. Eur J Radiol. 2011; 79(2):172–176. [PubMed: 20138721]
35. Sciarra A, Panebianco V, Ciccariello M, et al. Magnetic resonance spectroscopic imaging (1H-MRSI) and dynamic contrast-enhanced magnetic resonance (DCE-MRI): pattern changes from inflammation to prostate cancer. Cancer Invest. 2010; 28(4):424–432. [PubMed: 20073578]

36. Mohan H, Bal A, Punia RP, Bawa AS. Granulomatous prostatitis: an infrequent diagnosis. Int J Urol. 2005; 12(5):474–478. [PubMed: 15948747]
37. Oppenheimer JR, Kahane H, Epstein JI. Granulomatous prostatitis on needle biopsy. Arch Pathol Lab Med. 1997; 121(7):724–729. [PubMed: 9240909]
38. Stillwell TJ, Engen DE, Farrow GM. The clinical spectrum of granulomatous prostatitis: a report of 200 cases. J Urol. 1987; 138(2):320–323. [PubMed: 3599248]
39. Epstein JI, Hutchins GM. Granulomatous prostatitis: distinction among allergic, nonspecific, and post-transurethral resection lesions. Hum Pathol. 1984; 15(9):818–825. [PubMed: 6432674]
40. Maurice MJ, Zhu H. Sarcoidosis of the prostate. J Urol. 2013; 190(2):711–712. [PubMed: 23684704]
41. Mulpuru SK, Gujja K, Pai VM, Chen CY, Levey RL. A rare and unusual cause of PSA (prostate-specific antigen) elevation: sarcoidosis of the prostate. Am J Med Sci. 2008; 335(3):246–248. [PubMed: 18344703]
42. Furusato B, Koff S, McLeod DG, Sesterhenn IA. Sarcoidosis of the prostate. J Clin Pathol. 2007; 60(3):325–326. [PubMed: 17347286]
43. Wise GJ, Shteynshlyuger A. How to diagnose and treat fungal infections in chronic prostatitis. Curr Urol Rep. 2006; 7(4):320–328. [PubMed: 16930504]
44. Clason AE, McGeorge A, Garland C, Abel BJ. Urinary retention and granulomatous prostatitis following sacral herpes zoster infection: a report of 2 cases with a review of the literature. Br J Urol. 1982; 54(2):166–169. [PubMed: 7200822]
45. Bour L, Schull A, Delongchamps NB, et al. Multiparametric MRI features of granulomatous prostatitis and tubercular prostate abscess. Diagn Interv Imaging. 2013; 94(1):84–90. [PubMed: 23079151]
46. Gupta N, Mandal AK, Singh SK. Tuberculosis of the prostate and urethra: a review. Indian J Urol. 2008; 24(3):388–391. [PubMed: 19468474]
47. Zajaczkowski T. Genitourinary tuberculosis: historical and basic science review—past and present. Cent European J Urol. 2012; 65(4):182–187.
48. Wang LJ, Wong YC, Chen CJ, Lim KE. CT features of genitourinary tuberculosis. J Comput Assist Tomogr. 1997; 21(2):254–258. [PubMed: 9071295]
49. Reddy MN, Verma S. Lesions of the seminal vesicles and their MRI characteristics. J Clin Imaging Sci. 2014; 4:61. [PubMed: 25396077]
50. Alpern HD. Malakoplakia of the prostate. Int Urol Nephrol. 1991; 23(3):257–259. [PubMed: 1889972]
51. Blair JE, Maclennan GT. Malakoplakia. J Urol. 2005; 173(3):986. [PubMed: 15711361]
52. Prando A, Billis A. Focal prostatic atrophy: mimicry of prostatic cancer on TRUS and 3D-MRSI studies. Abdom Imaging. 2009; 34(2):271–275. [PubMed: 19374027]
53. De Visschere PJ, De Meerleer GO, Fütterer JJ, Villeirs GM. Role of MRI in follow-up after focal therapy for prostate carcinoma. AJR Am J Roentgenol. 2010; 194(6):1427–1433. [PubMed: 20489080]
54. Klimas R, Bennett B, Gardner WA Jr. Prostatic calculi: a review. Prostate. 1985; 7(1):91–96. [PubMed: 3909127]
55. Tamada T, Sone T, Jo Y, et al. Prostate cancer: relationships between postbiopsy hemorrhage and tumor detectability at MR diagnosis. Radiology. 2008; 248(2):531–539. [PubMed: 18539890]
56. Ikonen S, Kivisaari L, Vehmas T, et al. Optimal timing of post-biopsy MR imaging of the prostate. Acta Radiol. 2001; 42(1):70–73. [PubMed: 11167335]
57. Rosenkrantz AB, Kopec M, Kong X, et al. Prostate cancer vs. post-biopsy hemorrhage: diagnosis with T2- and diffusion-weighted imaging. J Magn Reson Imaging. 2010; 31(6):1387–1394. [PubMed: 20512891]
58. Barrett T, Vargas HA, Akin O, Goldman DA, Hricak H. Value of the hemorrhage exclusion sign on T1-weighted prostate MR images for the detection of prostate cancer. Radiology. 2012; 263(3): 751–757. [PubMed: 22474673]

59. Zakian KL, Shukla-Dave A, Ackerstaff E, Hricak H, Koutcher JA. 1H magnetic resonance spectroscopy of prostate cancer: biomarkers for tumor characterization. Cancer Biomark. 2008; 4(4–5):263–276. [PubMed: 18957715]

SA-CME LEARNING OBJECTIVES

After completing this journal-based SA-CME activity, participants will be able to:

- List the spectrum of anatomic and pathologic findings that mimic prostate carcinoma at multiparametric MR imaging.
- Describe the similarities and differences of the MR imaging findings between the mimics and prostate carcinoma.
- Discuss how the imaging features of the mimics correlate with the histopathologic findings.

See www.rsna.org/education/search/RG.

TEACHING POINTS

- The key histologic features of prostate carcinoma pertinent to MR imaging are increased cellular density, decreased luminal volume, reduced extracellular space, and neoangiogenesis.
- The normal central zone appears homogeneously hypointense on T2-weighted images and dark on ADC maps in patients aged 42–84 years. With these characteristics, it can mimic prostate cancer. A symmetric appearance of the central zone and its expected location can be helpful to differentiate it from prostate cancer, but in 20% of cases, the central zone may be asymmetric.
- Homogeneous low signal intensity (erased charcoal sign), ill-defined margins, lack of capsule, lenticular shape, and invasion of the anterior fibromuscular stroma are the MR imaging findings suggestive of transition zone cancer on T2-weighted images. Stromal hyperplasia tends to be more well defined, with a rounded encapsulated appearance.
- A clinical history of urinary and/or sexual symptoms, fluctuating PSA level, or PSA response to antibiotics can alert the radiologist and the clinician to the possibility of prostatitis.
- Florid granulomatous prostatitis may demonstrate extraprostatic extension. In patients with a histologic diagnosis of granulomatous prostatitis and prostate cancer, it is difficult to predict whether the findings of extraprostatic extension are secondary to prostate cancer or to granulomatous disease, since both entities may have a similar appearance at MR imaging.

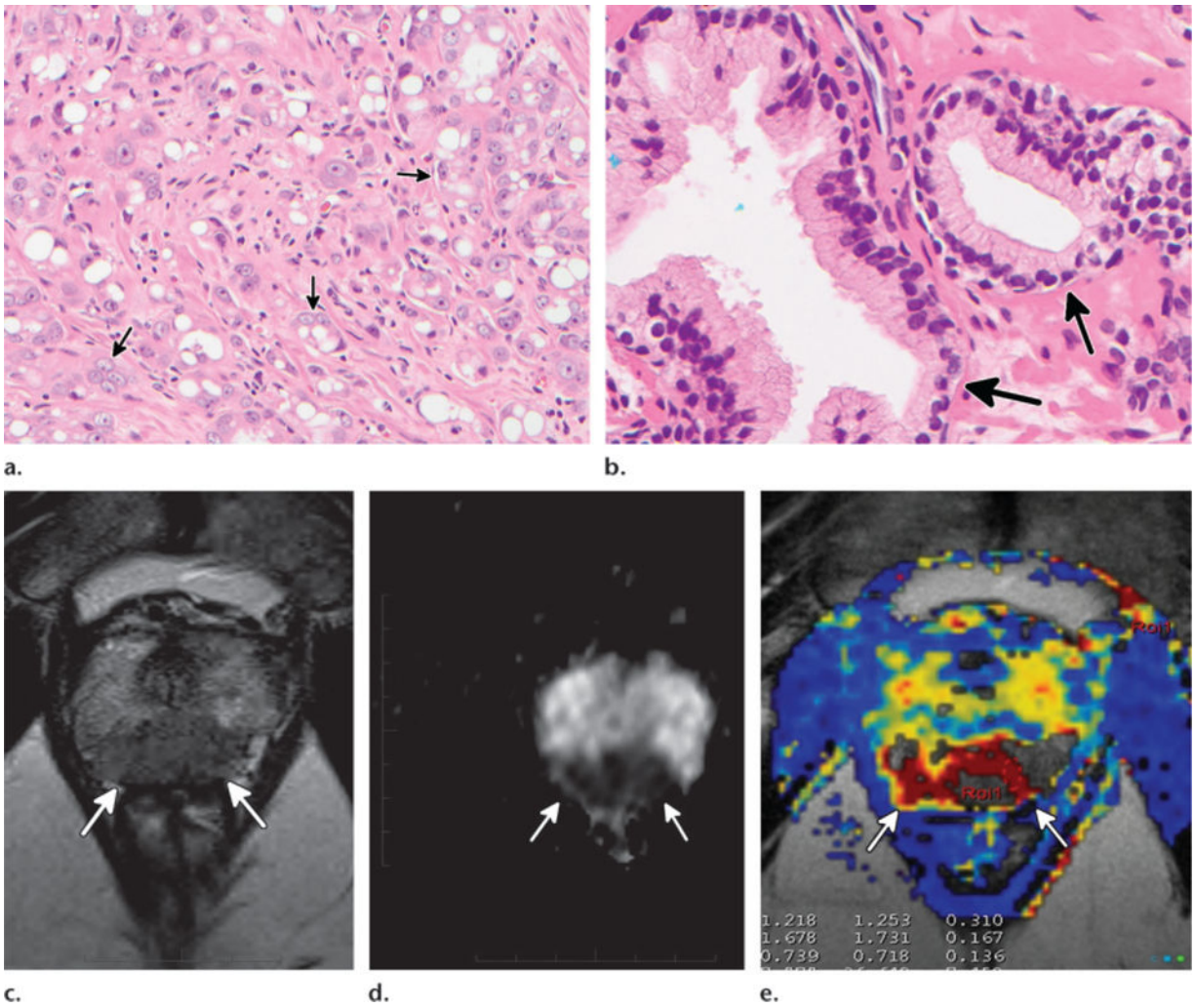

Figure 1.

Histologic and multiparametric MR imaging findings in prostate carcinoma. **(a, b)** High-power photomicrographs show poorly differentiated grade 5 prostate carcinoma with dispersed nests of carcinoma cells (arrows in **a**) and normal peripheral zone glandular tissue with well-formed glands (arrows in **b**). (Original magnification, ×200; hematoxylin-eosin [H-E] stain.) **(c–e)** Axial T2-weighted image **(c)**, axial apparent diffusion coefficient (ADC) map **(d)**, and axial k^{trans} image **(e)** show characteristic multiparametric MR imaging findings of high-grade (Gleason 8) prostate carcinoma in the midline apical peripheral zone (arrows).

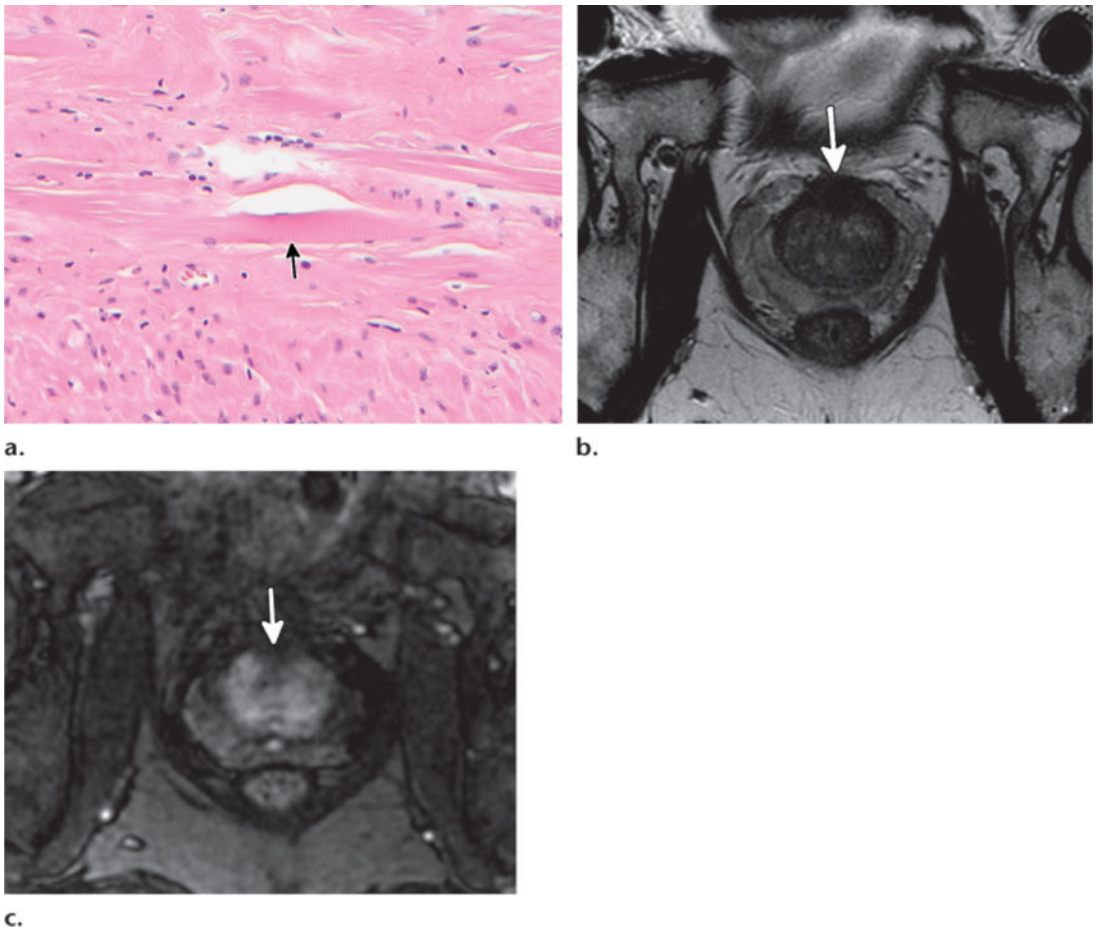

Figure 2.
Histologic and multiparametric MR imaging findings of the anterior fibromuscular stroma. **(a)** High-power photomicrograph shows fibromuscular tissue interspersed with skeletal muscle fibers (arrow). (Original magnification, ×200; H-E stain.) **(b, c)** Axial T2-weighted **(b)** and DCE **(c)** images show normal anterior fibromuscular stroma, which is T2 hypointense and hypovascular (arrow).

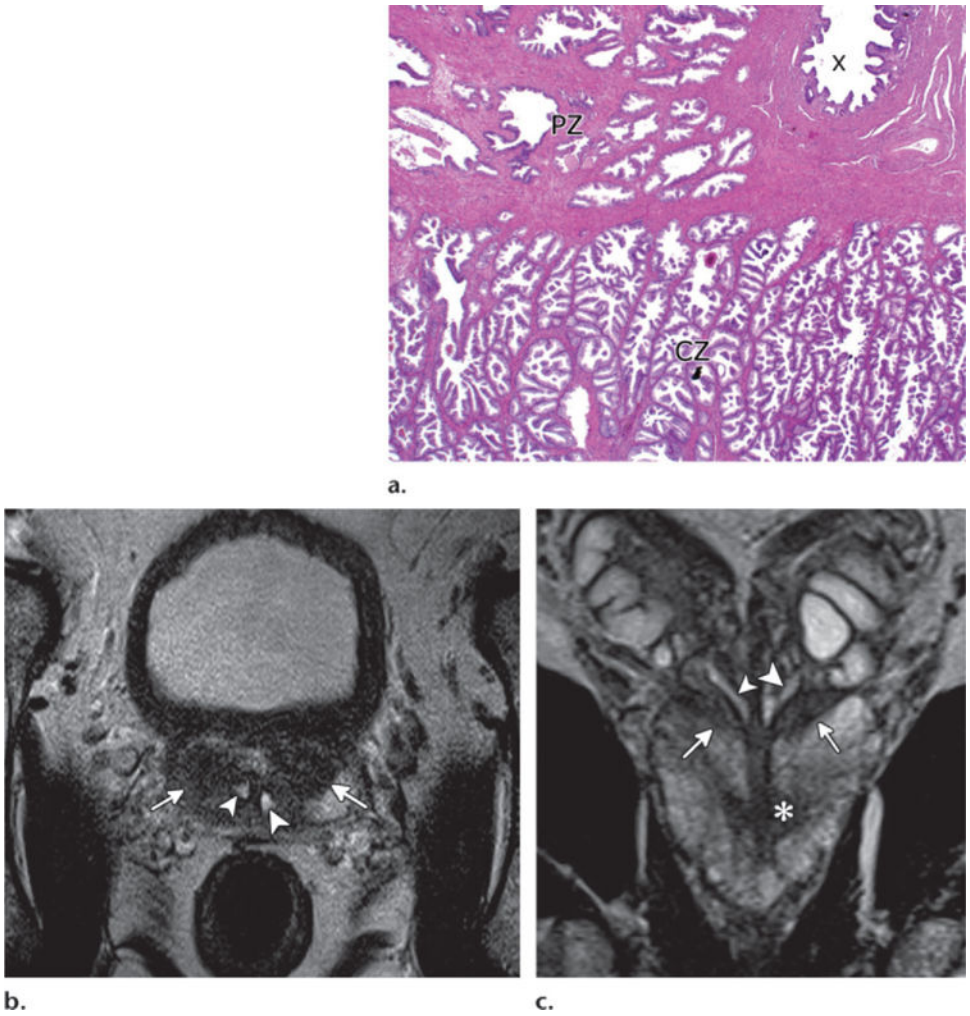

Figure 3.

Histologic and multiparametric MR imaging findings of the central zone. **(a)** Low-power photomicrograph shows the central zone *(CZ)* with complex glandular architecture compared to the more sparse simple glands of the peripheral zone (*PZ*). The central zone is close to the adjacent ejaculatory duct *(X)* surrounded by fibromuscular tissue. (Original magnification, ×20; H-E stain.) **(b, c)** Axial **(b)** and coronal **(c)** T2-weighted images show the normal symmetric central zone (arrows) adjacent to the ejaculatory ducts (arrowheads) in a 61-year-old man with Gleason 7 cancer (* in **c**).

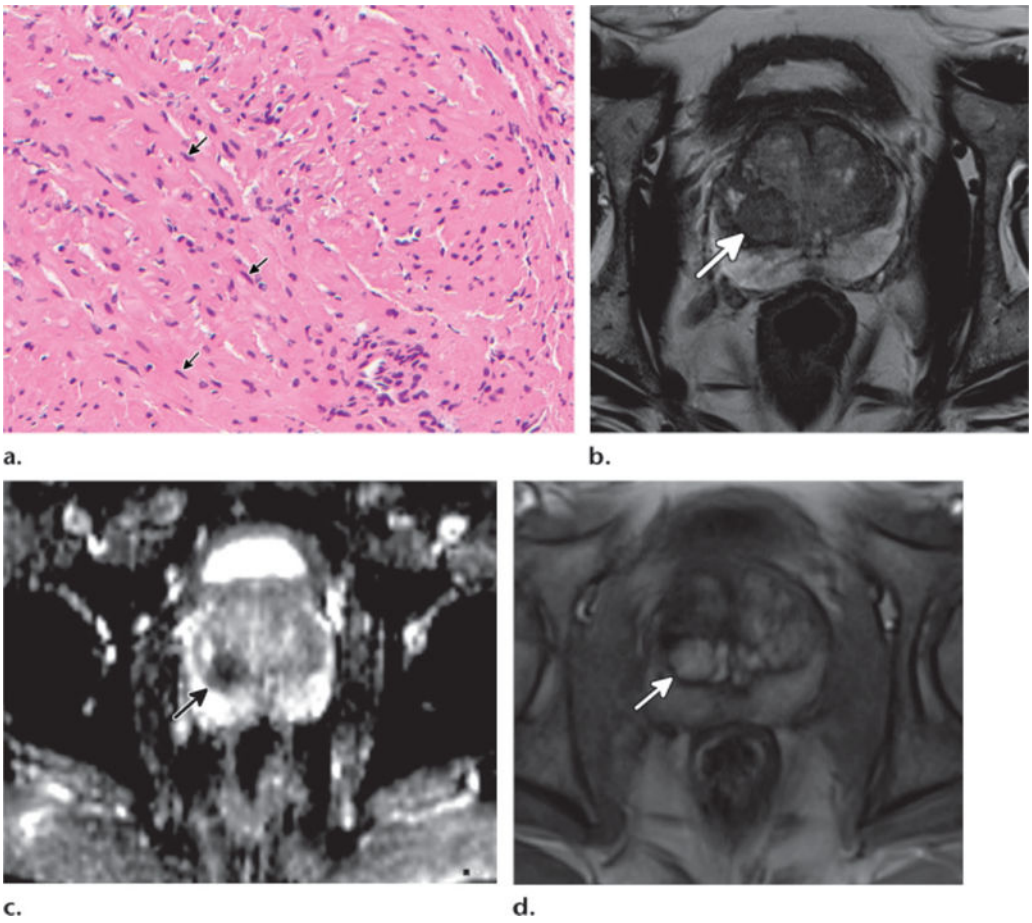

Figure 4.
Stroma-rich BPH nodule confirmed with MR imaging–guided biopsy in a 58-year-old man. **(a)** High-power photomicrograph of MR imaging–guided biopsy specimen shows stroma-rich BPH with proliferation of mesenchymal spindle cells (arrows) and absence of glandular tissue. (Original magnification, ×200; H-E stain.) **(b–d)** Axial T2-weighted image **(b)**, axial ADC map **(c)**, and axial DCE image **(d)** show a well-defined nodule (arrow) in the right transition zone with low T2 signal intensity, diffusion restriction, and hyperenhancement.

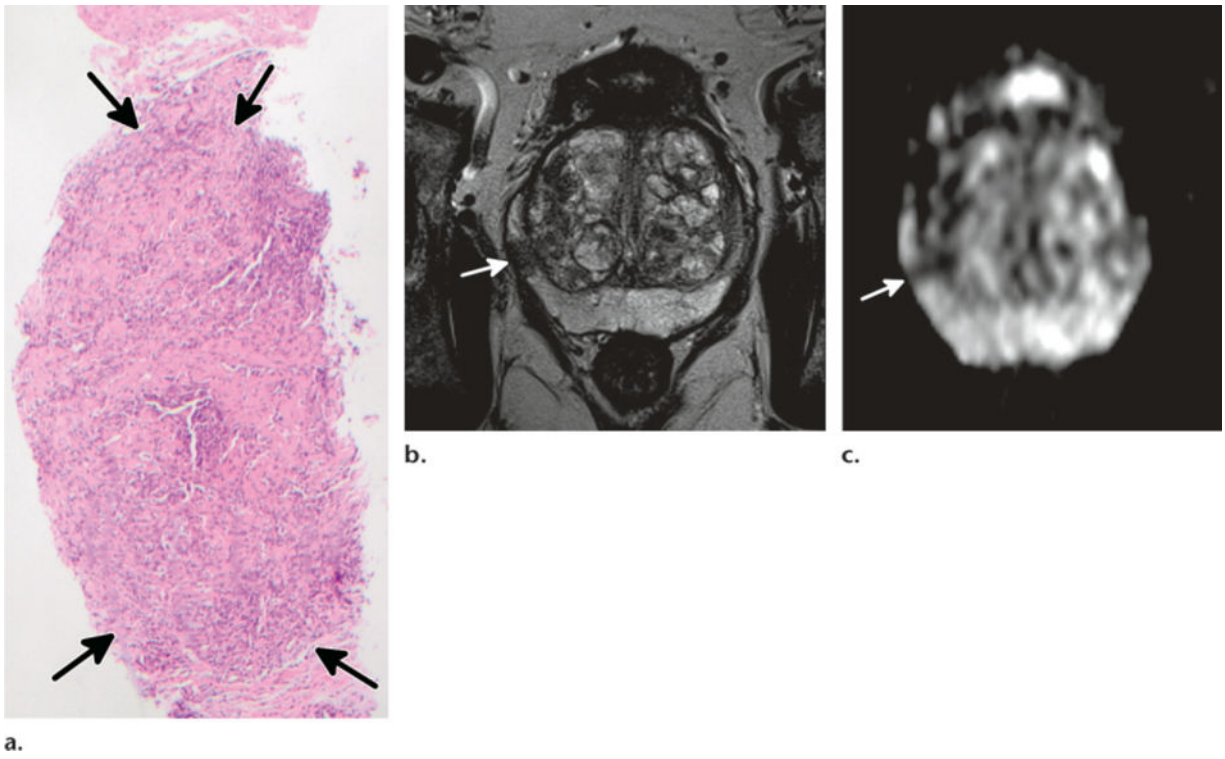

Figure 5.

Nodular acute prostatitis confirmed with MR imaging–guided biopsy in a 69-year-old man. **(a)** Low-power photomicrograph of MR imaging–guided biopsy specimen shows acute prostatitis with a nodular area (arrows) of predominantly neutrophil infiltration. (Original magnification, ×20; H-E stain.) **(b, c)** Axial T2-weighted image **(b)** and axial ADC map **(c)** show a rounded nodule (arrow) in the right peripheral zone with diffusion restriction and moderate enhancement (not shown).

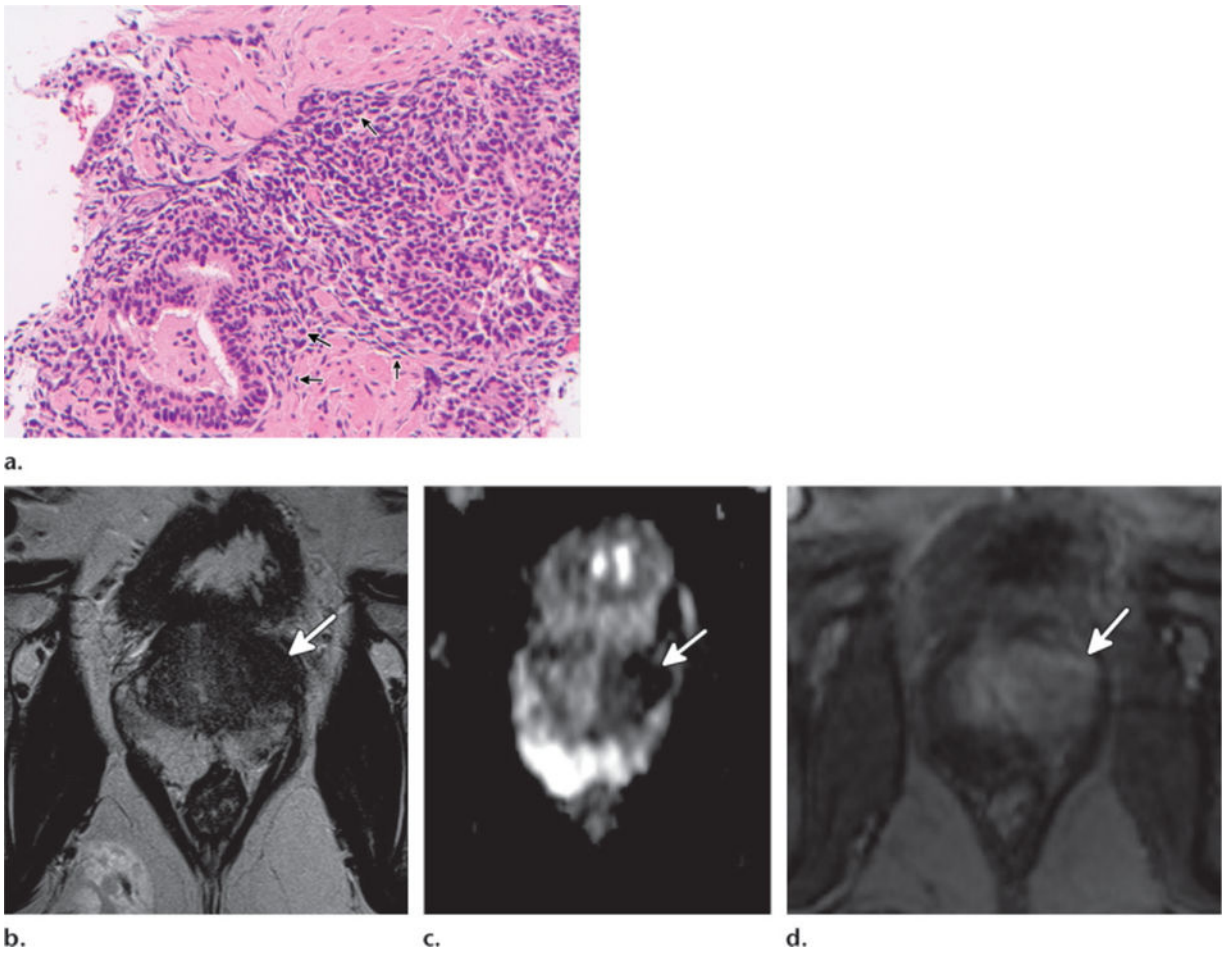

Figure 6.
Focal chronic prostatitis of the transition zone confirmed with MR imaging–guided biopsy in a 62-year-old man. **(a)** High-power photomicrograph of MR imaging–guided biopsy specimen shows extensive lymphocyte infiltration (arrows), in keeping with chronic prostatitis. (Original magnification, ×200; H-E stain.) **(b–d)** Axial T2-weighted image **(b)**, axial ADC map **(c)**, and axial DCE image **(d)** show a low-signal-intensity mass (arrow) in the left transition zone with diffusion restriction and early rapid enhancement.

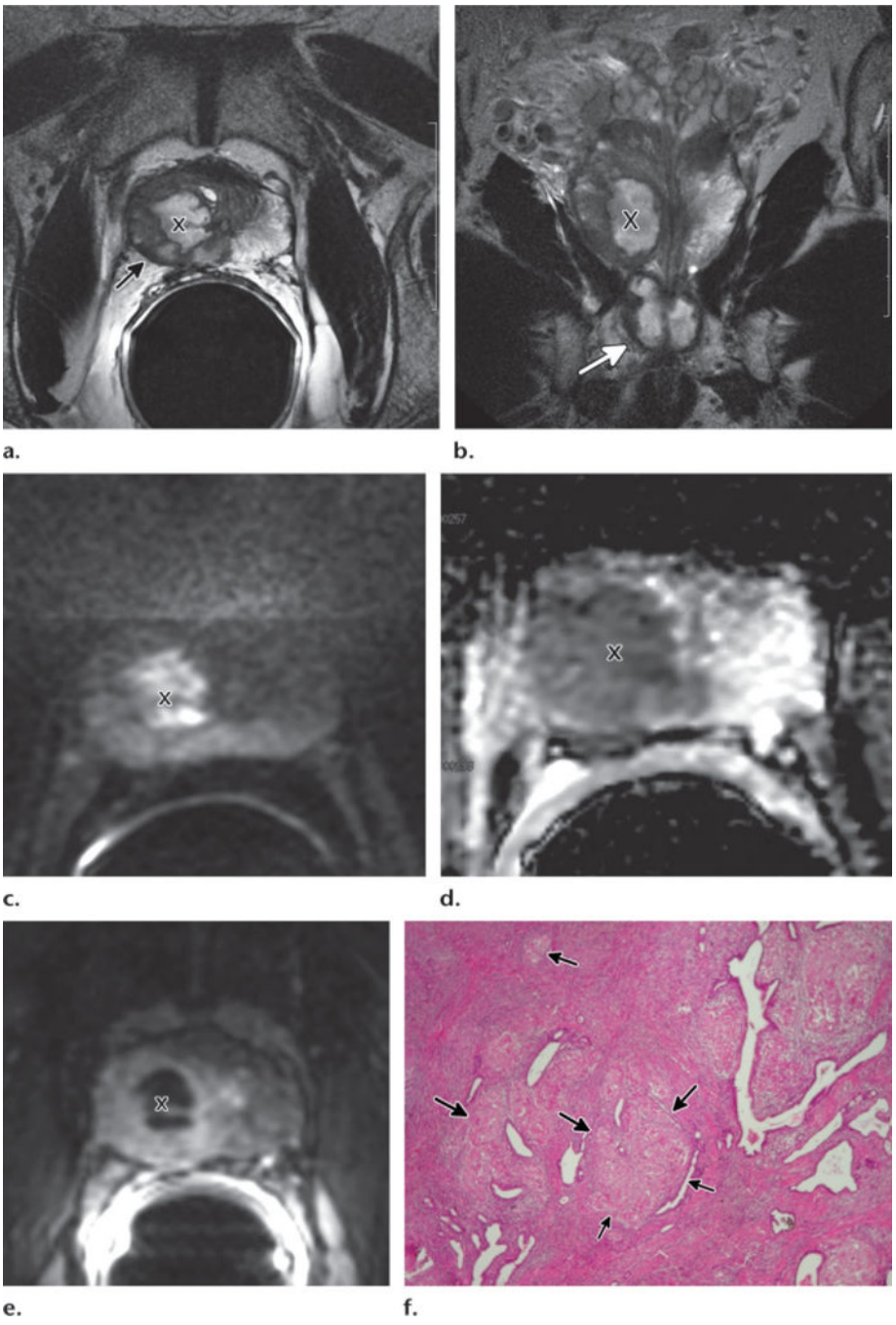

Figure 7.

Necrotic (caseating) mycobacterial granulomatous prostatitis and prostate cancer in a 64-year-old man with rising PSA level 2 years after completing intravesical bacillus Calmette-Guérin therapy. Transrectal US–guided biopsy revealed Gleason 6 prostate cancer and granulomatous prostatitis in the right lobe. **(a–e)** Axial T2-weighted image **(a)**, coronal T2-weighted image **(b)**, axial DW image **(c)**, axial ADC map **(d)**, and axial DCE image **(e)** show cavitating mycobacterial granulomatous prostatitis with extraprostatic extension. Cavitation *(X)* appears as high signal intensity on the T2-weighted images, hyperintensity on

the high-*b*-value DW image, low ADC, and lack of enhancement. The abscess is surrounded by granulomatous infiltration, which appears as low T2 signal intensity, diffusion restriction, and moderate enhancement. The caseating process shows extraprostatic extension on the axial T2-weighted image with capsular irregularity and bulging (arrow in **a**). It also extends through the apex of the prostate (arrow in **b**) on the coronal T2-weighted image. **(f)** Low-power photomicrograph shows inflammation with granuloma formation (arrows). (Original magnification, ×40; H-E stain.)

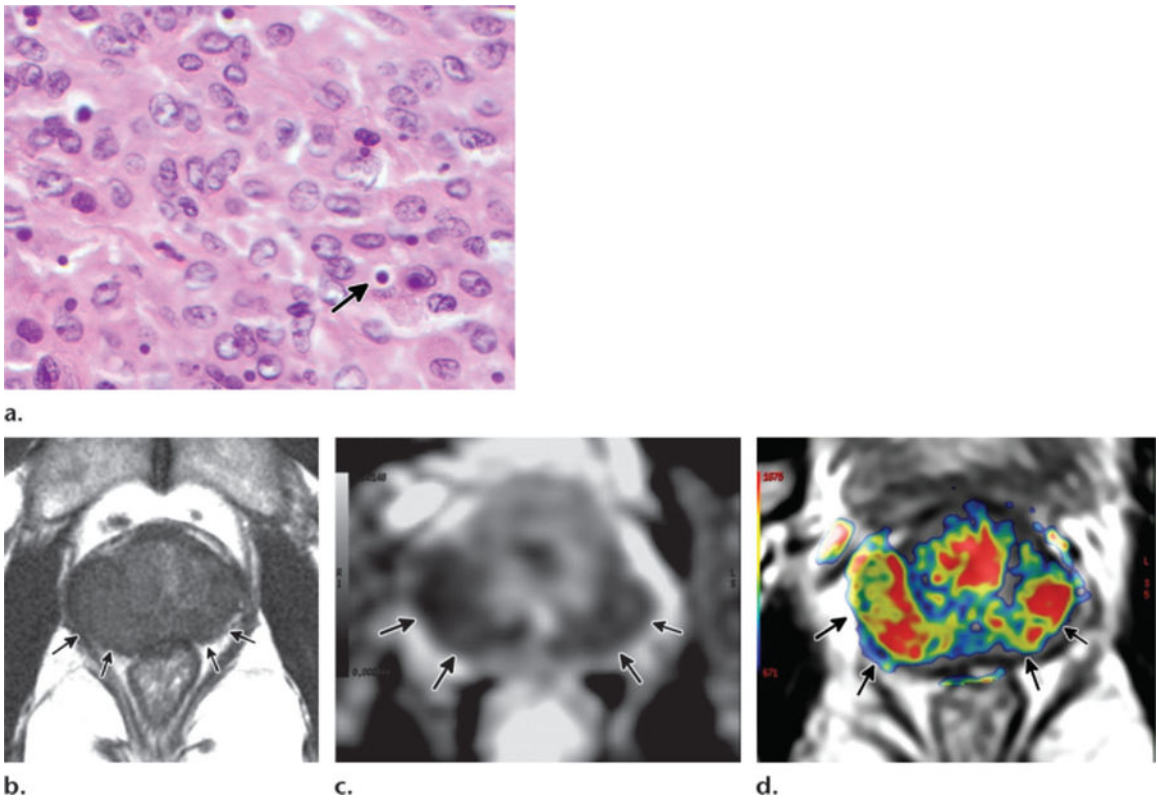

Figure 8.

Malacoplakia in a 49-year-old man with recurrent episodes of acute prostatitis 6 months earlier and elevated PSA level. Transrectal US–guided biopsy showed malacoplakia. **(a)** High-power photomicrograph shows inflammatory infiltrate with pathognomonic intracellular Michaelis-Gutmann inclusion bodies (arrow). (Original magnification, ×600; H-E stain.) **(b–d)** Axial T2-weighted image **(b)**, axial ADC map **(c)**, and axial K^{trans} image **(d)** show diffuse peripheral zone abnormality (arrows) with low T2 signal intensity, low ADC, and enhancement.

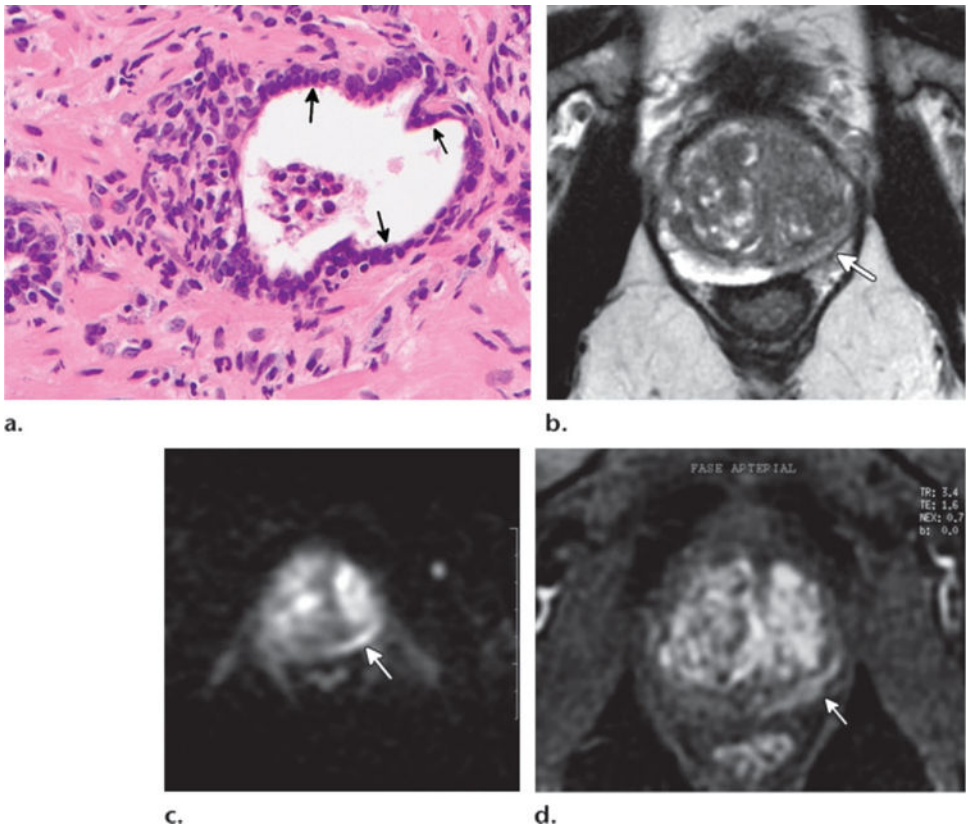

Figure 9.

Focal prostatic atrophy in a 65-year-old man with a history of progressively elevated PSA level and three previous negative biopsies. Repeat biopsy targeting the MR imaging–identified region showed atrophy. **(a)** High-power photomicrograph shows prostatic atrophy changes with glands of well-formed open lumina lined by cells with scant cytoplasm and hyperchromatic nuclei (arrows). (Original magnification, ×400; H-E stain.) **(b–d)** Axial T2-weighted **(b)**, axial DW **(c)**, and axial DCE **(d)** images show left peripheral zone geographic low T2 signal intensity with mild volume loss, diffusion restriction, and enhancement (arrow).

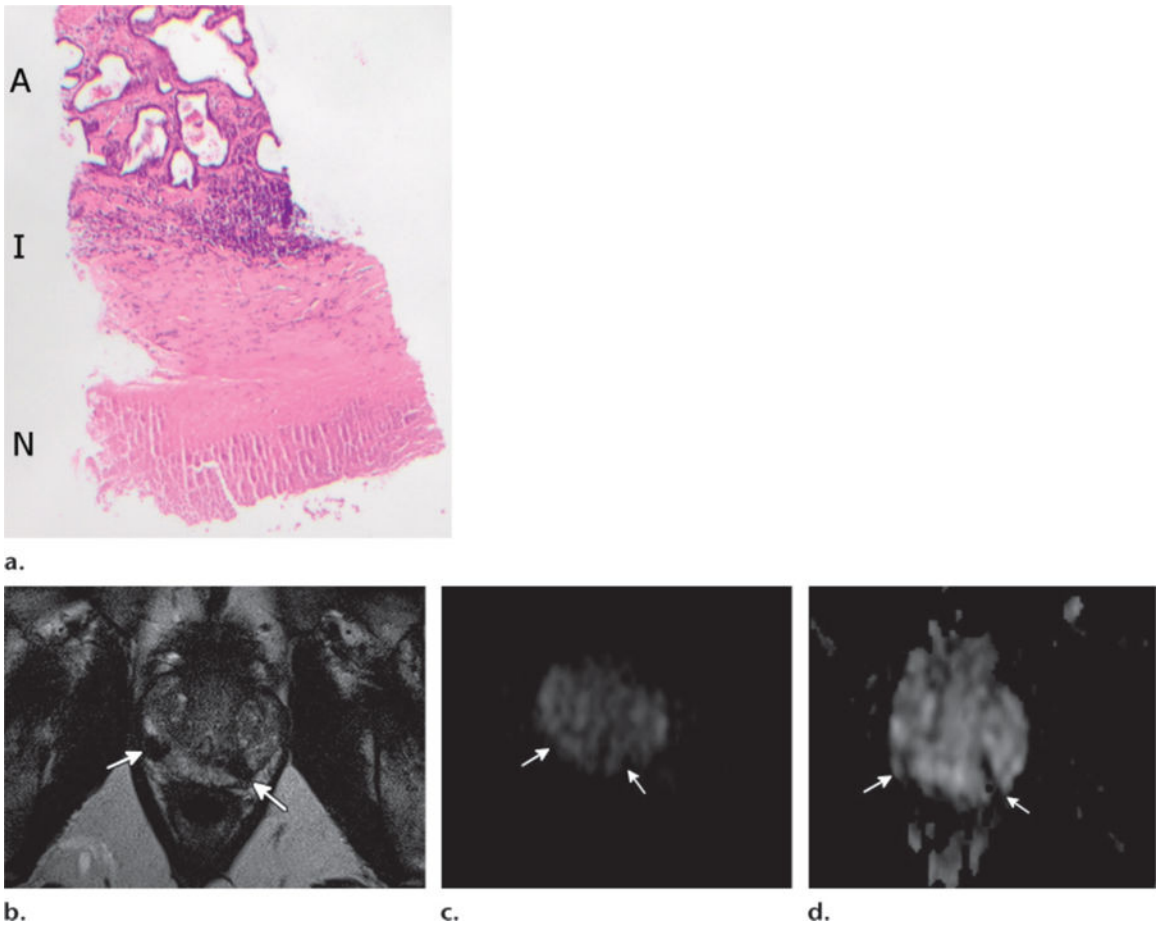

Figure 10.

Prostatic necrosis and atrophy in a 58-year-old man with bacillus Calmette-Guérin vaccine–related granulomatous prostatitis 3 years earlier with subsequent treatment but ongoing elevation of PSA level. MR imaging–guided biopsy showed necrosis and atrophy. **(a)** Low-power photomicrograph shows a zonation effect of central necrosis *(N)*, peripheral inflammatory infiltrate *(I)*, and atrophy *(A)*. (Original magnification, ×10; H-E stain.) **(b–d)** Axial T2-weighted image **(b)**, axial high-*b*-value DW image **(c)**, and axial ADC map **(d)** show two areas of markedly low T2 signal intensity in the peripheral zone (arrows). These areas have low signal intensity on the high-*b*-value DW image, low ADC, and nonenhancement (not shown).

Table 1

Sample MR Imaging Parameters for Evaluation of the Prostate

Sequence and Orientation	TR/TE(msec)	Field of View (mm)	Matrix	Section Thickness (mm)
T2-weighted FSE				
Axial	3300/96	180.0 × 180.0	320 × 320	3.0
Coronal	3300/96	180.0 × 180.0	320 × 288	3.0
Sagittal	3300/96	180.0 × 180.0	320 × 320	3.0
Axial T1-weighted SE	776/10	319.0 × 284.0	384 × 274	4.0
Axial single-shot EP DW (b = 50, 600, and 1200 sec/mm^2)	4700/90	189.0 × 220.0	134 × 200	3.0
Axial 3D GRE T1-weighted DCE (temporal resolution, 5.8 sec)	4.83/1.87	259.0 × 259.0	133 × 192	3.3

Note.—Performed at 3 T with a pelvic phased-array coil and no endorectal coil. There may be variation of the parameters between the three centers involved in this article. EP = echo-planar, FSE = fast spin-echo, GRE = gradient-echo, SE = spin-echo, 3D = three-dimensional, TR/TE = repetition time/echo time.

Table 2

Benign Conditions That Mimic Prostate Carcinoma at MR Imaging

Conditions	Histologic and Anatomic Features
Anatomic	
Anterior fibromuscular stroma	Dense fibromuscular band anterior to the transition zone
Surgical capsule	Band of fibromuscular and compressed glandular tissue between the transition zone and peripheral zone
Central zone	Complex crowded glands and dense stroma surrounding the ejaculatory ducts
Periprostatic vein	Venous plexus closely associated with the pseudocapsule
Periprostatic lymph nodes	Lymph nodes adjacent to the lateral or posterolateral prostate
Benign pathologic	
Stroma-rich BPH	Stromal fibromuscular proliferation in the transition zone and occasionally in the peripheral zone
Bacterial prostatitis (acute or chronic)	Inflammatory (neutrophils or lymphocytes) infiltrate with or without glandular atrophy
Mycobacterial granulomatous prostatitis	Granulomatous inflammation with or without central caseation
Malacoplakia	Granulomatous inflammation with Michaelis-Gutmann bodies
Atrophy	Crowded glands with scant cytoplasm and nuclear crowding
Necrosis	Coagulative necrosis with surrounding chronic inflammatory infiltrate and atrophy
Calcification	Concreted prostatic secretions or calcified corpora amylacea
Hemorrhage	Hemorrhage